Published online 30 April 2022

Nucleic Acids Research, 2022, Vol. 50, No. 9 ***5129–5144***
https://doi.org/10.1093/nar/gkac304

SCF ubiquitin E3 ligase regulates DNA double-strand breaks in early meiotic recombination

Yongjuan Guan[1], Huijuan Lin[1,2], N. Adrian Leu[1], Gordon Ruthel[3], Serge Y. Fuchs[1], Luca Busino[4], Mengcheng Luo[2] and P. Jeremy Wang[1,*]

[1]Department of Biomedical Sciences, University of Pennsylvania School of Veterinary Medicine, Philadelphia, PA, USA, [2]Department of Tissue and Embryology, Hubei Provincial Key Laboratory of Developmentally Originated Disease, School of Basic Medical Sciences, Wuhan University, Wuhan, Hubei Province, China, [3]Department of Pathobiology, University of Pennsylvania School of Veterinary Medicine, Philadelphia, PA, USA and [4]Department of Cancer Biology, University of Pennsylvania Perelman School of Medicine, Philadelphia, PA, USA

Received January 07, 2022; Revised April 08, 2022; Editorial Decision April 13, 2022; Accepted April 14, 2022

ABSTRACT

Homeostasis of meiotic DNA double strand breaks (DSB) is critical for germline genome integrity and homologous recombination. Here we demonstrate an essential role for SKP1, a constitutive subunit of the SCF (SKP1-Cullin-F-box) ubiquitin E3 ligase, in early meiotic processes. SKP1 restrains accumulation of HORMAD1 and the pre-DSB complex (IHO1-REC114-MEI4) on the chromosome axis in meiotic germ cells. Loss of SKP1 prior to meiosis leads to aberrant localization of DSB repair proteins and a failure in synapsis initiation in meiosis of both males and females. Furthermore, SKP1 is crucial for sister chromatid cohesion during the pre-meiotic S-phase. Mechanistically, FBXO47, a meiosis-specific F-box protein, interacts with SKP1 and HORMAD1 and targets HORMAD1 for polyubiquitination and degradation in HEK293T cells. Our results support a model wherein the SCF ubiquitin E3 ligase prevents hyperactive DSB formation through proteasome-mediated degradation of HORMAD1 and subsequent modulation of the pre-DSB complex during meiosis.

INTRODUCTION

In sexually reproducing organisms, homologous chromosomes undergo meiotic recombination to exchange genetic materials (1,2,3). As a key driver of genetic diversity in gametes, meiotic recombination plays a paramount role in evolution of species. Meiotic recombination begins with formation of many programmed meiotic DNA double-strand breaks (DSBs) in germ cells. The number and location of meiotic DSBs are tightly controlled. Absence of DSBs leads to recombination failure and ensuing sterility. However, an excess of DSBs is deleterious to the germline genome integrity and interferes with the meiotic recombination process. Abnormality in meiotic recombination leads to infertility, aneuploidy-related birth defects, and pregnancy loss.

Formation of meiotic DSBs is catalyzed by the SPO11 and TOPOVIBL DNA topoisomerase enzyme complex (4,5,6). Meiotic recombination occurs at a high frequency at certain genomic locations, known as hotspots, which are specified by PRDM9-catalyzed H3K4me3 marks (7,8,9). Cytologically, DSBs are formed on the chromosome axis that will later form the lateral elements of the synaptonemal complex (SC). HORMAD1 localizes to unsynapsed chromosome axis and recruits the pre-DSB complex (IHO1–REC114–MEI4), which promotes formation of SPO11-catalyzed DSBs (10). DSBs are resected to produce ∼1 kb-long 3′ single-strand DNA (ssDNA) overhangs, which are bound by the ssDNA-binding protein RPA (11,12). The ssDNA-binding recombinases DMC1 and RAD51 replace RPA and drive ssDNA invasion into the homologous chromosome (13,14). The BRCA2–HSF2BP–BRME1 complex promotes recruitment of RAD51/DMC1 to DSBs (15,16,17). MEIOB and SPATA22 form a meiosis-specific ssDNA-binding complex that interacts with RPA and are possibly involved in second end capture (18,19,20,21). Second end capture results in formation of double Holliday junctions (dHJ), resolution of which leads to crossovers. Meiotic recombination is executed stepwise by a large number of enzymes, DNA-binding proteins, and chromatin-remodeling factors. Fidelity of this process is paramount for preservation of fertility and genetic inheritance.

In mice, hundreds of DSBs are generated in each meiotic germ cell and fewer than 10% of them lead to the formation of ∼22 crossovers per cell. The number and location of meiotic DSBs are tightly regulated locally and globally (22). Normally, formation of one DSB suppresses the formation of others nearby, presumably because formation of two adjacent DSBs on the same chromatid would lead

*To whom correspondence should be addressed. Tel: +1 215 746 0160; Email: pwang@vet.upenn.edu

to a deletion of the intervening genomic region. In addition, formation of a second DSB in proximity on the homologous chromosome would interfere with homologous recombination, as neither homologue would be intact to serve as a repair template. The ATM kinase is essential for meiosis in mice (23,24). *Atm*-deficient meiotic germ cells show increased formation of DSBs (12,22,25,26). While ATM acts as one known regulator of meiotic DSB formation, the control of DSB homeostasis remains poorly understood.

The SCF (SKP1–Cullin–F-box) ubiquitin E3 ligase is a large family of E3 enzymes. Each SCF E3 ligase is composed of four subunits: SKP1, CUL1, the RING finger protein RBX1 and an F-box protein. SKP1 (S-phase kinase-associated protein 1) interacts with each of 69 mammalian F-box proteins to form distinct E3 ligase complexes to target specific protein substrates for degradation (27,28,29). The SCF E3 ligase controls many cellular processes such as cell cycle progression, transcription, signal transduction, and tumorigenesis. *Skp1* is a ubiquitously expressed essential gene and its global deletion is embryonic lethal (30). SKP1 was initially identified as a key regulator of cell cycle (31) and later found in a proteomics screen for meiotic chromatin-associated proteins (18). SKP1 localizes to the synapsed regions of homologous chromosomes in meiotic germ cells (30). Inducible deletion of *Skp1* in meiotic cells in adult mice reveals that SKP1 is essential for maintenance of chromosomal synapsis and the cell cycle progression from the meiotic prophase I to metaphase I (30). Here, we have identified a novel role for the SCF E3 ligase in meiotic DSB formation and repair. We inactivated *Skp1* in spermatogonia, prior to meiotic initiation, using *Stra8*-Cre. All analyses in spermatocytes were performed on juvenile mice. Meiotic cells deficient in *Skp1* exhibited abnormal accumulation of HORMAD1 and the pre-DSB complex on meiotic chromatins and failed to form chromosomal synapsis. The ssDNA-binding DSB repair proteins were mislocalized in *Skp1*-deficient meiotic cells. Importantly, FBXO47, an F-box protein, interacted with HORMAD1 and facilitated polyubiquitination of HORMAD1. Collectively, this study uncovers an unexpected role for the SCF ubiquitin E3 ligase in regulation of meiotic DSB homeostasis.

MATERIALS AND METHODS

Mouse strains

The *Skp1*^{fl} mice were generated previously (30). We obtained *Spo11*$^{+/-}$ mice (Stock No: 019117) from the Jackson Laboratory (5,32). We also obtained cryopreserved sperm from *Hormad1*$^{+/-}$ mice (MMRRC Stock No: 41469-JAX) from the Jackson Laboratory (33). ICSI was performed to generate *Hormad1*$^{+/-}$ mice at PennVet Transgenic Core facility. *Stra8*-Cre mice were generated previously (34). Genotyping was performed by PCR with tail genomic DNA using primers in Supplementary Table S1. Mice were maintained and used according to the guidelines of the Institutional Care and Use Committee of the University of Pennsylvania.

Histological, immunofluorescence and surface nuclear spread analyses

For histological analysis, testes or ovaries were fixed in Bouin's solution at room temperature overnight, embedded with paraffin, and sectioned. Sections were stained with hematoxylin and eosin. For immunofluorescence, testes were fixed in 4% paraformaldehyde (in 1× PBS) for 6 h at 4°C, dehydrated in 30% sucrose (in 1× PBS) overnight, and prepared for cutting cryosections. Surface nuclear spread analysis was reported before (30). Briefly, testicular tubules or oocytes were soaked in hypotonic treatment buffer (30 mM Tris, 50 mM sucrose, 17 mM trisodium citrate dihydrate, 5 mM EDTA, 0.5 mM DTT, 1 mM PMSF). The cells were suspended in 100 mM sucrose and then spread on PTFE printed slides (Cat. No. 63418-11, Electron Microscopy Sciences) that were pre-soaked with paraformaldehyde solution containing Triton X-100 and sodium borate. The primary antibodies used for immunofluorescence were listed in Supplementary Table S2.

Imaging

Histological images were captured on the Leica DM5500B microscope with a DFC450 digital camera (Leica Microsystems). Most immunolabeled chromosome spread images were taken on a Leica DM5500B microscope with an ORCA Flash4.0 digital monochrome camera (Hamamatsu Photonics). Confocal microscopy of immunolabeled chromosome spreads was performed on a Leica SP5 II confocal (Leica Microsystems, Mannheim, Germany) with a 100× (1.46 NA) oil immersion objective lens. Images were deconvolved with Huygens Essential deconvolution software (Scientific Volume Imaging B.V., Hilversum, Netherlands).

Western blot analysis

Testes or ovaries were homogenized in 3 volumes of protein extraction buffer [62.5 mM Tris–HCl (pH 6.8), 3% SDS, 10% glycerol, 5% 2-mercaptoethanol]. Samples were then boiled at 95°C for 10–15 min. A total of 20 μg of protein samples were resolved by SDS-PAGE and transferred onto nitrocellulose membranes using iBlot (Invitrogen).

Cell culture and transfection

HEK293T cells were maintained in DMEM/high glucose (Mediatech) supplemented with 10% FBS (Sigma-Aldrich) and penicillin/streptomycin (Invitrogen). Plasmid DNA transfections in HEK293T cells were carried out using lipofectamine 2000 (Invitrogen). For each well of a 6-well plate, 2–4 μg of plasmids and 8 μl of lipofectamine 2000 (Invitrogen) were used for transfection. Cells were collected 24–36 h after transfection for further analysis. For MG132 (Sigma) treatment experiment, 24 h after transfection, the cells were treated with MG132 (10 μM) for 4 hours before collection.

Co-immunoprecipitation and immunoblotting assays

1×10^7 cells were collected after transfection for *in vitro* co-immunoprecipitation. Cells were lysed in 1 ml RIPA

buffer (10 mM Tris, pH 8.0, 140 mM NaCl, 1% Trion X-100, 0.1% sodium deoxycholate, 0.1% SDS, 1 mM EDTA) supplemented with 1 mM PMSF. For immunoprecipitation (IP), cell lysates were centrifuged by 16 000 g for 30 min at 4°C, and 1.5% of the supernatant was set aside as input. The remaining lysates were pre-cleared with 15 μl protein G Dynabeads (Thermo Fisher Scientific) for 2 h, and then incubated with 2 μg primary antibodies at 4°C for 1 h. The lysates were then incubated with 30 μl protein G Dynabeads overnight. The immunoprecipitated complexes were washed with RIPA buffer three times and boiled in 30 μl 2× SDS-PAGE loading buffer at 95°C for 10 min. 20 μl of the supernatant was resolved by SDS-PAGE. For immunoblotting analysis, the resolved proteins were transferred onto a nitrocellulose membrane using iBlot (Invitrogen) and immunoblotted with primary and secondary antibodies (Supplementary Table S2).

Ubiquitination assay

FLAG-FBXO47, MYC-FLAG-FBXW8, MYC-FLAG-FBXW17, MYC-FLAG-FBXO28, V5-HORMAD1 and HA-ubiquitin expression plasmids were co-transfected into HEK293T cells (Supplementary Table S3). After 24 h, 10 μm MG132 (M8699, Sigma) was added and incubated for 4 h to inhibit proteasome. Transfected cells were lysed with the RIPA buffer supplemented with 1 mM PMSF. Cell lysates were incubated with mouse anti-V5 antibody (R960-25, Invitrogen) at 4°C overnight and then incubated with Dynabeads G at 4°C for 3 h. The precipitants were washed three times with the RIPA buffer and followed by western blot analysis with mouse anti-HA antibody (12CA5, Roche) and rabbit anti-HORMAD1 antibody (13917-1-AP, Proteintech).

RESULTS

SKP1 is essential for synapsis initiation during male meiosis

To assess the potential role of *Skp1* in early meiosis, we conditionally inactivated *Skp1* before the onset of meiosis by generating *Skp1*$^{fl/-}$*Stra8*-Cre mice (referred to as *Skp1*^{cKO}) (Supplementary Figure S1). The *Stra8*-Cre is expressed in both male and female germ cells prior to meiosis (Supplementary Figure S1) (34,35). Adult *Skp1*^{cKO} testis was much smaller than wild type (*Skp1*$^{fl/+}$) testis (Figure 1A). The *Skp1*^{cKO} testis weight was reduced by 78% (Figure 1B). Western blot showed that the SKP1 protein was nearly absent in the 8-week-old *Skp1*^{cKO} testis (Figure 1C). Germ cells of different developmental stages appear at definite times in wild type juvenile testes, with the appearance of pachytene spermatocytes at postnatal day 16 (P16) and round spermatids at P21 (Figure 1D). However, *Skp1*^{cKO} testes lacked post-meiotic spermatids and displayed complete meiotic arrest at P16, P21, and P56 (Figure 1D). To determine the stage of meiotic arrest in *Skp1*^{cKO} testes, we performed immunofluorescence analysis of SYCP1 (SC central/transverse filaments) and SYCP3 (SC lateral elements) in spread nuclei of spermatocytes. While SYCP1 marked the synapsed regions in wild type (*Skp1*$^{fl/+}$, no Cre) zygotene and pachytene spermatocytes, *Skp1*^{cKO} spermatocytes lacked SYCP1 signals, showing that SKP1 is required for formation of chromosomal synapsis (Figure 1E and F). In the most advanced *Skp1*^{cKO} spermatocytes, chromosome axial elements were well formed but synapsis was absent. These cells were referred to as zygotene-like spermatocytes, as they lacked synapsis. Therefore, in addition to the previously reported requirement of SKP1 in the maintenance of chromosomal synapsis (30), these results demonstrate that SKP1 plays an essential role in the initiation of chromosomal synapsis.

SKP1 is critical for sister chromatid cohesion

Notably, abnormal spermatocytes with apparently separated sister chromatids were found in *Skp1*^{cKO} testis and thus referred to as leptotene-like (Figure 1E). The leptotene-like cells accounted for 20% of spermatocytes in *Skp1*^{cKO} testis but were absent in *Skp1*$^{fl/+}$ testis (Figure 1F). To further examine this defect, we counted the number of CREST foci (centromeres) (Figure 1G and H). Because of chromosomal synapsis, the number of CREST foci is reduced from 40 in leptotene/zygotene spermatocytes to 21 in pachytene spermatocytes (the XY centromeres are separate). Consistent with a failure in synapsis initiation, *Skp1*^{cKO} zygotene-like spermatocytes contained 40 CREST foci. However, the average number of CREST foci in *Skp1*^{cKO} leptotene-like cells was 65, with a range from 42 to 138, showing severe defects in sister chromatid cohesion. The DNA content of *Skp1*^{cKO} leptotene cells was similar to that of wild type leptotene cells, suggesting the occurrence of pre-meiotic S-phase DNA replication (Supplementary Figure S2A). The presence of >40 CREST foci in *Skp1*^{cKO} leptotene-like cells further supported the occurrence of pre-meiotic DNA replication. We next examined the localization of cohesins (Supplementary Figure S2B and C). REC8 and STAG3 are meiosis-specific cohesins and both localize to the chromosome axes of sister chromatids (36,37,38). REC8 and STAG3 still formed filaments in *Skp1*^{cKO} leptotene-like cells, which overlapped with the SYCP3 filaments (Supplementary Figure S2B and C). Collectively, these results show that SKP1 plays a role in sister chromatid cohesion.

SKP1 restrains pre-DSB complex formation

We next sought to investigate the process of meiotic recombination in *Skp1*^{cKO} spermatocytes. In wild type spermatocytes, HORMAD1 localizes to chromosome axes as filaments at the leptotene stage and to unsynapsed axes at the zygotene stage (Figure 2A). In contrast, HORMAD1 accumulates more dramatically on the unsynapsed axes in *Skp1*-deficient spermatocytes at all stages (leptotene, leptotene-like, and zygotene-like) (Figure 2A). In juvenile testes, meiosis proceeds in a defined timeline. Spermatocytes first progress to preleptotene/leptotene stages at P10, the zygotene stage at P12, and the pachytene stage at P14. Western blot analysis using the whole testicular lysates revealed that the SKP1 protein was still abundant in *Skp1*^{cKO} testis at P10, but was severely depleted in *Skp1*^{cKO} testes at P12, P14 and P60 (adult) (Figure 3D). The residual SKP1 protein in *Skp1*^{cKO} testes was presumably from progenitor spermatogonia and testicular somatic cells where *Stra8*-Cre was not expressed. The abundance of HORMAD1 was comparable between *Skp1*^{cKO} and *Skp1*$^{fl/+}$ testes at postnatal day

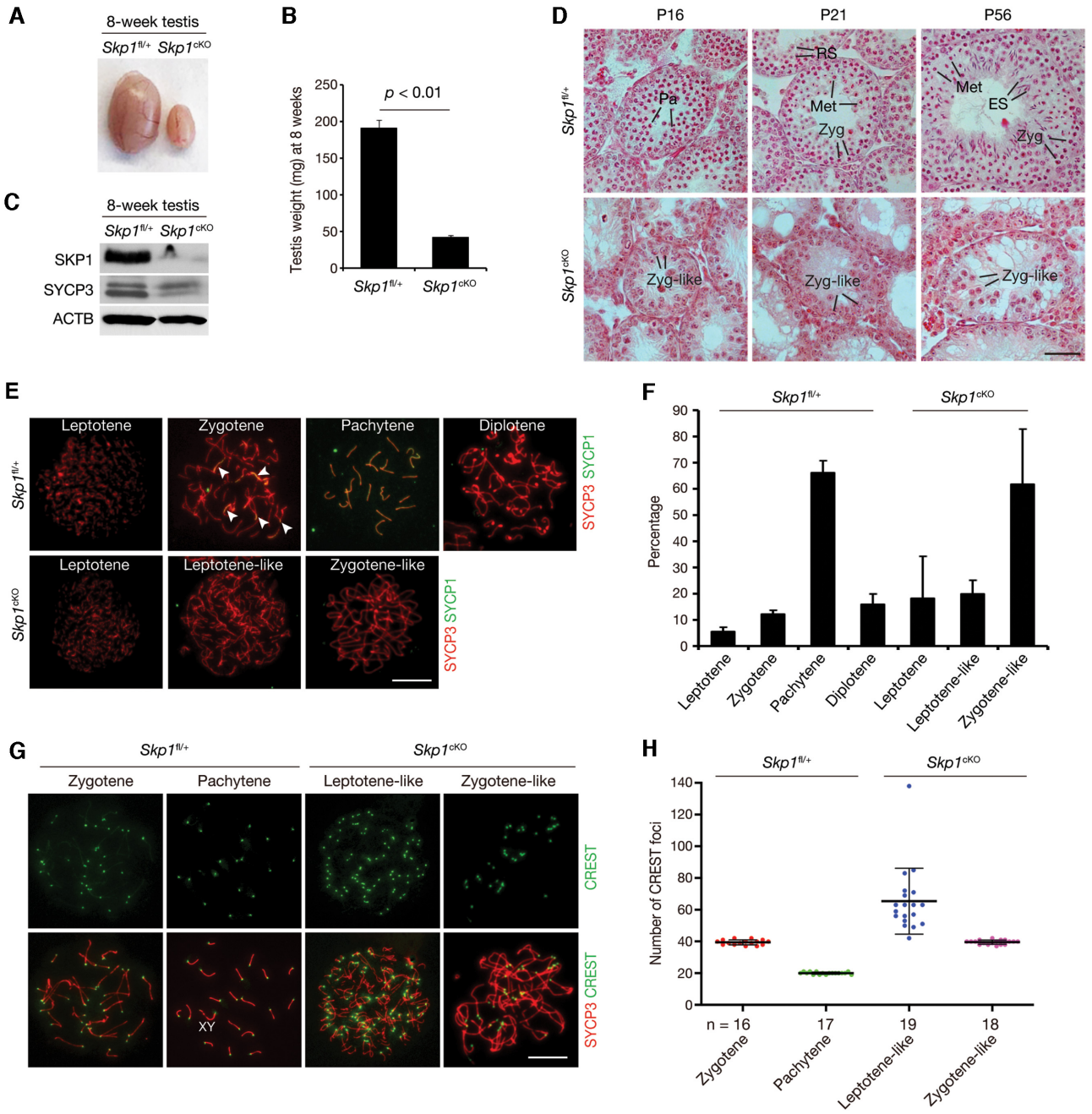

Figure 1. SKP1 is essential for chromosomal synapsis and sister chromatid cohesion in male meiosis. (**A**) Reduced testis size in 8-week-old *Skp1*^{cKO} males. (**B**) Reduced testis weight in 8-week-old *Skp1*^{cKO} males ($n = 3$). Value = mean ± s.d. (**C**) Western blot analysis of SKP1 in 8-week-old testes. SYCP3 and ACTB serve as a meiosis-specific control and a loading control respectively. (**D**) Histology of testes from *Skp1*$^{fl/+}$ and *Skp1*^{cKO} males at postnatal days 16, 21 and 56. Zyg, zygotene; Zyg-like, zygotene-like; Pa, pachytene; Met, metaphase; RS, round spermatids; ES, elongated spermatids. Scale bar, 50 μm. (**E**) Surface nuclear spread analysis of *Skp1*$^{fl/+}$ and *Skp1*^{cKO} spermatocytes from P20 testes. Arrowheads indicate regions of synapsis (SYCP1-positive) in *Skp1*$^{fl/+}$ zygotene cells. Scale bar, 10 μm. (**F**) The percentage of each type of spermatocytes in *Skp1*$^{fl/+}$ and *Skp1*^{cKO} P20 testes. Value = mean ± s.d. 180–220 cells per mouse and three mice per genotype were analyzed. (**G**) Immunofluorescence of centromeres in *Skp1*$^{fl/+}$ and *Skp1*^{cKO} spermatocytes from P20 testes. Scale bar, 10 μm. (**H**) The plot shows the number of CREST foci in *Skp1*$^{fl/+}$ and *Skp1*^{cKO} spermatocytes from P20 testes.

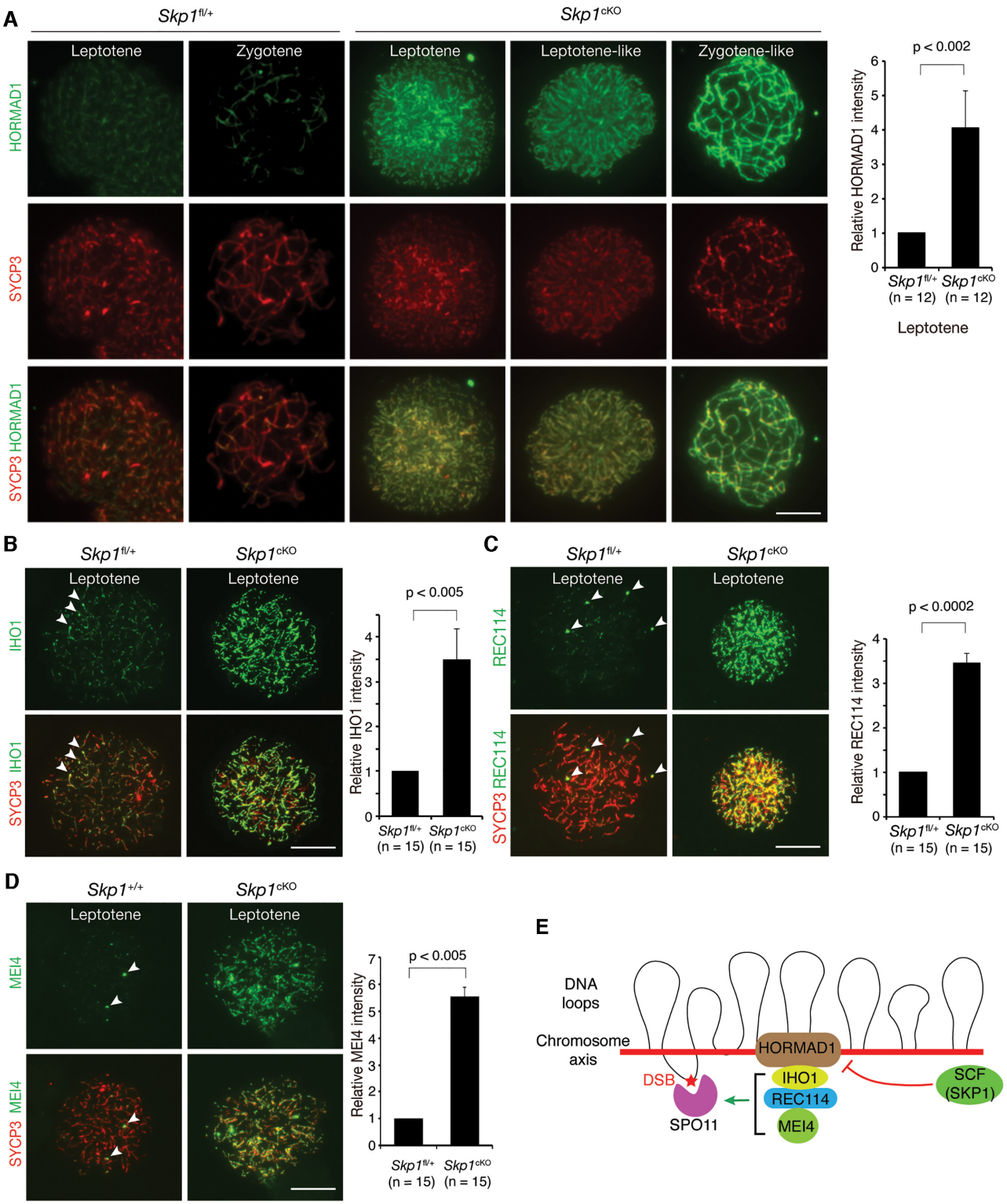

Figure 2. SKP1 restrains accumulation of HORMAD1 and the pre-DSB complex on the chromosome axis. (**A**) Excessive accumulation of HORMAD1 on unsynapsed axes in *Skp1*^{cKO} spermatocytes from P20 testes. (**B**) Increased intensity of IHO1 foci in *Skp1*^{cKO} leptotene cells from P20 testes. (**C**) Increased intensity of REC114 foci in *Skp1*^{cKO} leptotene cells from P20 testes. (**D**) Increased intensity of MEI4 foci in *Skp1*^{cKO} leptotene cells from P20 testes. In the graphs, fluorescent signals of HORMAD1, IHO1, REC114 and MEI4 were normalized to SYCP3 signals, and the values were set at 1.0 in *Skp1*$^{fl/+}$ cells. *n*, number of leptotene cells. Value = mean ± s.d. The *P* values were calculated by Student's *t*-test. Scale bars, 10 μm. White arrowheads in *Skp1*$^{fl/+}$ leptonema indicate the large IHO1 blobs (B), REC114 blobs (C) and MEI4 blobs (D), which are known sites of mo-2 minisatellite arrays (39). (**E**) Working model of regulation of meiotic DSB homeostasis by SCF^{SKP1}.

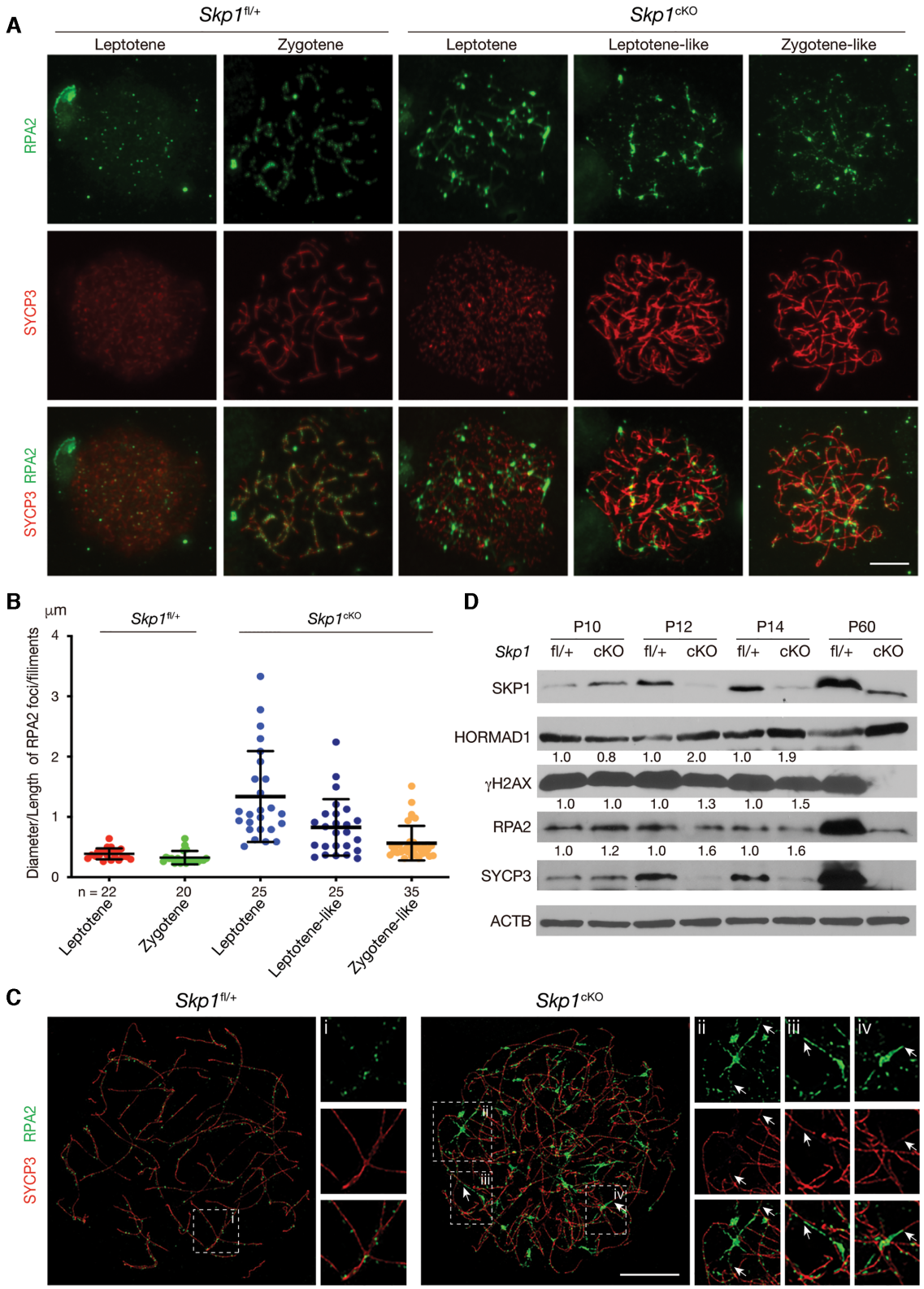

Figure 3. Aberrant focal and filamentous localization of RPA2 in *Skp1*^{cKO} spermatocytes. (**A**) Immunofluorescence of RPA2 in *Skp1*$^{fl/+}$ and *Skp1*^{cKO} spermatocytes from P20 testes with anti-RPA2 and anti-SYCP3 antibodies. Scale bar, 10 μm. (**B**) The size of RPA2 foci in *Skp1*$^{fl/+}$ and *Skp1*^{cKO} spermatocytes from P20 testes. The diameter/length of each focus or fiber was measured with ImageJ. (**C**) Confocal microscopy of RPA2 and SYCP3 in *Skp1*$^{fl/+}$ zygotene spermatocytes and *Skp1*^{cKO} leptotene-like spermatocytes from P20 testes. Enlarged images of the boxed areas (i-iv) are shown. Arrows indicate the junctions of RPA2 fibers and SYCP3 filaments in *Skp1*^{cKO} cells. Scale bar, 10 μm. (**D**) Western blot analysis of SKP1, HORMAD1, γH2AX, RPA2 and SYCP3 in *Skp1*^{cKO} and *Skp1*$^{fl/+}$ testes. The relative abundance of HORMAD1, γH2AX and RPA2 is normalized to SYCP3. The value in *Skp1*$^{fl/+}$ testes is set at 1.0. Quantification was not performed for P60, because SYCP3 was not detectable in P60 *Skp1*^{cKO} testis. ACTB serves as a loading control.

10 (P10) but sharply increased in *Skp1*^{cKO} testes at P12 and beyond (Figure 3D). HORMAD2 also accumulated more substantially on the chromosome axis in *Skp1*^{cKO} spermatocytes (Supplementary Figure S3A and B). At the leptotene stage, HORMAD1 recruits the IHO1-REC114-MEI4 pre-DSB complex to the chromosome axis, which promotes DSB formation by SPO11 (10). IHO1, REC114 and MEI4 formed foci on the chromosome axis in wild type leptotene cells and these foci were of much higher intensity in *Skp1*^{cKO} leptotene cells (Figure 2B–D). Quantification of fluorescence intensity showed that the signals of HORMAD1, IHO1, REC114 and MEI4 were increased by 3 to 6 folds in *Skp1*^{cKO} leptotene cells compared to *Skp1*$^{fl/+}$ cells (Figure 2). Notably, the large IHO1, REC114 or MEI4 blobs are known to correspond to the mo-2 minisatellite regions (Figure 2B–D) (39). Collectively, these data support that SKP1 restrains the accumulation of HORMAD1 and thus the pre-DSB complexes on the chromosome axis (Figure 2E).

ssDNA-binding proteins form abnormal foci and fibers in *Skp1*-deficicent cells

We next examined the effect of *Skp1* deficiency on DSB formation and repair. DSB leads to phosphorylation of H2AX by ATM (40). Notably, γH2AX was present in *Skp1*-deficient spermatocytes, indicating that meiotic DSBs were generated (Supplementary Figure S3C). We next examined the effect of *Skp1* deficiency on localization of RPA, which binds to resected ssDNA. RPA2 is one of the three subunits of the RPA complex (11). We found four abnormal localization patterns of RPA2 in *Skp1*-deficient spermatocytes (Figure 3A–C). First, RPA2 foci were present in all *Skp1*$^{fl/+}$ zygotene spermatocytes ($n = 212$ cells from four P20 mice), however, 92% of *Skp1*^{cKO} zygotene-like spermatocytes had RPA2 foci, but the remaining 8% lacked RPA2 foci ($n = 197$ cells from four P20 mice). Second, RPA2 foci were much larger and more intense in *Skp1*^{cKO} spermatocytes than in *Skp1*$^{fl/+}$ spermatocytes (Figure 3A). While RPA2 foci in *Skp1*$^{fl/+}$ cells were small and relatively uniform in size, RPA2 foci in *Skp1*^{cKO} spermatocytes were variable in size with some being very large (Figure 3A). Specifically, *Skp1*^{cKO} leptotene cells had the largest RPA2 foci, followed by leptotene-like and zygotene-like spermatocytes (Figure 3B). The number of RPA2 foci was lower in *Skp1*^{cKO} leptotene cells, possibly due to the presence of unusually large foci (Supplementary Figure S4A). Third, while RPA2 foci were always present on the chromosome axis in *Skp1*$^{fl/+}$ cells, most RPA2 foci did not localize to the chromosome axis in *Skp1*^{cKO} cells, indicating that DSBs might be formed on DNA loops (Figure 3A). Fourth, *Skp1*^{cKO} spermatocytes contained RPA2 thread-like fibers, which were connected to large foci in a spider-web-like pattern, whereas such RPA fibers were never observed in *Skp1*$^{fl/+}$ meiotic cells (Figure 3C). Confocal microscopy revealed that each large RPA2 focus in *Skp1*^{cKO} spermatocytes was a single RPA aggregate but not a cluster of small foci (Figure 3C). In addition, the thin RPA2 fibers emanating from the large RPA2 aggregate/focus were often connected to the SYCP3 filaments in *Skp1*^{cKO} spermatocytes (Figure 3C). The dramatically enlarged RPA2 foci and the formation of RPA2 fibers in *Skp1*^{cKO} spermatocytes indicate dysregulated DSB processing and possible abnormal DSB end resection.

We examined the abundance of γH2AX and RPA2 in *Skp1*^{cKO} and wild type testes at postnatal day 10, 12, 14 and 60 by western blotting analysis (Figure 3D). The abundance of γH2AX and RPA2 was normalized to SYCP3 to account for the reduced number of meiotic cells in *Skp1*^{cKO} testes due to the early meiotic arrest. The abundance of γH2AX and RPA2 was increased in *Skp1*^{cKO} testes at P12 and P14, in comparison with the *Skp1*$^{fl/+}$ testes, indicating increased DSB breaks or impaired DSB processing in *Skp1*^{cKO} testes.

To further evaluate the process of meiotic recombination, we examined other ssDNA-binding proteins including MEIOB, SPATA22, DMC1 and RAD51. The MEIOB/SPATA22 complex interacts with RPA and are required for meiotic recombination (18,19,20,21,41). DNA recombinases RAD51 and DMC1 drive strand invasion into homologous DNA duplex during meiosis (13,14,42,43). Interestingly, foci of these four proteins were also much larger and more intense in *Skp1*^{cKO} spermatocytes and these proteins also formed long thread-like fibers (Figure 4A-D). The number of DMC1 foci and RAD51 foci was mostly increased in *Skp1*^{cKO} spermatocytes (Supplementary Figure S4B and C). The large RPA2 foci and SPATA22 foci nearly always overlapped, whereas ∼60% of RPA2 and DMC1 foci overlapped (Supplementary Figure S4D). The BRCA2–HSF2BP–BRME1 complex recruits RAD51/DMC1 to DSBs (15,16,17). HSF2BP and BRME1 were assembled as foci in wild type spermatocytes (Figure 4E and F). Larger foci of HSF2BP and BRME1 were formed in *Skp1*^{cKO} leptotene-like and zygotene-like cells (Figure 4E and F). Notably, the percentage of zygotene-like cells with foci for each of these proteins examined was reduced in *Skp1*^{cKO} testis (Supplementary Figure S4E). Taken together, these results reveal defects in early meiotic recombination in *Skp1*^{cKO} spermatocytes.

Synapsis failure in *Skp1*-deficient oocytes

In our previous study, we used *Ddx4*-Cre to inactivate *Skp1* in female germ cells and found that SKP1 was required to maintain chromosomal synapsis in pachytene oocytes but the 2-month-old *Skp1* conditional knockout (*Ddx4*-Cre) ovaries still contained oocytes (30). *Ddx4*-Cre begins expression at embryonic day 15 (E15), when oocytes are at the pachytene stage (Supplementary Figure S1) (44). To investigate an earlier role for *Skp1* in female meiosis, we employed *Stra8*-Cre. *Stra8* is expressed in female germ cells from E12.5, one day before meiotic onset (Supplementary Figure S1) (35). Therefore, the *Skp1*$^{fl/-}$*Stra8*-Cre (*Skp1*^{cKO}) mutant allowed us to elucidate the function of SKP1 at an earlier meiotic stage. Wild type (*Skp1*$^{fl/+}$) ovaries at P16 and P42 contained many follicles at various stages (Figure 5A). The *Skp1*^{cKO} ovaries at P16 and P42 were much smaller. Histological analysis showed that oocytes were present at a substantially reduced number in the *Skp1*^{cKO} ovaries at P16 but were absent in the mutant ovaries at P42 (Figure 5A). Immunofluorescence analysis using YBX2 as a marker of oocytes (45) and oocyte counts revealed a sharply reduced number of oocytes in the *Skp1*^{cKO} ovary at postnatal day one (P1) in comparison with the wild-type ovary

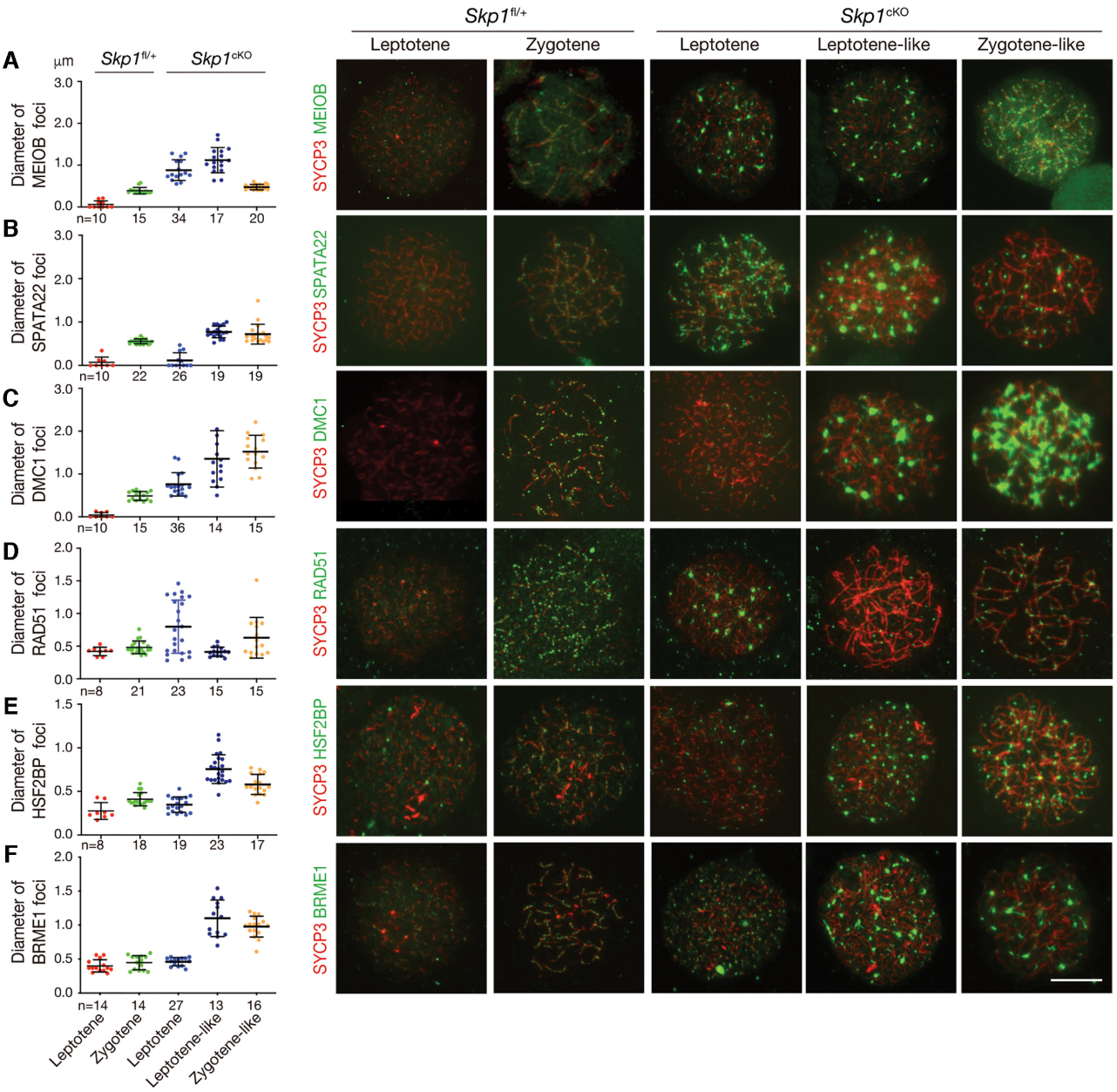

Figure 4. Aberrant localization of DSB repair proteins in *Skp1*^{cKO} spermatocytes. (A–F) Immunofluorescence analysis of MEIOB (**A**), SPATA22 (**B**), DMC1 (**C**), RAD51 (**D**), HSF2BP (**E**) and BRME1 (**F**) in *Skp1*$^{fl/+}$ and *Skp1*^{cKO} spermatocytes from P20 testes. The plot shows the diameter of foci or length of filaments in spermatocytes. Scale bar, 10 μm.

(Figure 5B). These results demonstrate that SKP1 is required for survival of postnatal oocytes.

The early loss of oocytes in the *Skp1*^{cKO} ovary at P1 is indicative of early meiotic defects (46). To monitor the progression of early meiosis in *Skp1*^{cKO} females, we studied embryonic ovaries. The levels of *Skp1* mRNA and SKP1 protein were substantially reduced in E16.5 *Skp1*^{cKO} ovaries (Supplementary Figure S5A and B). To examine chromosomal synapsis, we performed immunofluorescence analysis of SYCP1 and SYCP3 in spread nuclei of oocytes at E16.5. While SYCP1 localized to the synapsed regions of SC in *Skp1*$^{fl/+}$ zygotene oocytes as expected, SYCP1 was absent in zygotene-like oocytes from the *Skp1*^{cKO} ovaries, indicating a failure in synapsis initiation (Figure 5C). Homologous chromosomes were fully synapsed in *Skp1*$^{fl/+}$ pachytene oocytes, however, the most advanced oocytes in the *Skp1*^{cKO} ovaries were pachytene-like cells, in which homologous chromosomes were aligned but exhibited severe synapsis defects and very weak signals of SYCP1 (Figure 5C). SYCE1, a component of SC central elements, also exhibited weak signals in *Skp1*^{cKO} pachytene-like oocytes (Supplementary Figure S5C) (47,48). Quantification showed that most oocytes at E16.5 were pachytene cells in *Skp1*$^{fl/+}$ ovaries and pachytene-like cells in *Skp1*^{cKO} ovaries (Figure 5D). These results suggest that SKP1 is critical for synapsis initiation in female meiosis. Therefore, the requirement

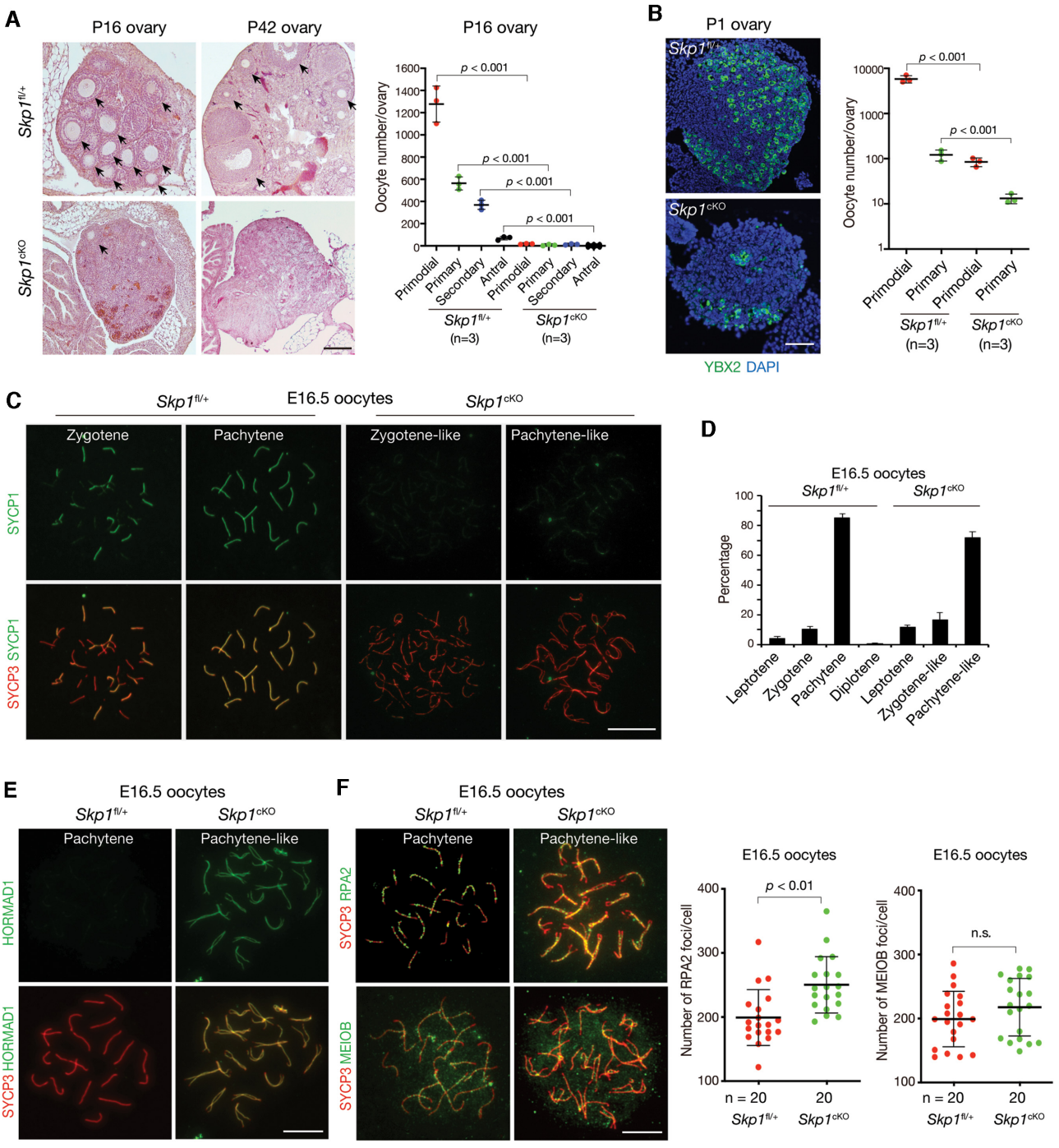

Figure 5. SKP1 is essential for synapsis formation during female meiosis. (**A**) Histological analysis of ovaries from P16 and P42 mice. Arrows indicate follicles at different stages. Scale bar, 50 μm. The plot shows the total number of follicles per P16 ovary: primordial, primary, secondary, and antral follicles. The oocyte count was performed as previously described (78). (**B**) Immunofluorescence of oocytes in P1 *Skp1*$^{fl/+}$ and *Skp1*^{cKO} ovaries. YBX2 is a marker of oocytes. Scale bar, 50 μm. The plot shows the total number of follicles per P1 ovary, which was counted based on histological sections as in panel A. (**C**) Surface nuclear spread analysis of *Skp1*$^{fl/+}$ and *Skp1*^{cKO} E16.5 oocytes with anti-SYCP1 and anti-SYCP3 antibodies. Scale bar, 10 μm. (**D**) The plot shows the percentage of each type of oocytes. 130–150 oocytes per mouse (two *Skp1*$^{fl/+}$ mice) and 120–150 oocytes per mouse (two *Skp1*^{cKO} mice) were counted. (**E**) Immunofluorescence of HORMAD1 in *Skp1*$^{fl/+}$ and *Skp1*^{cKO} E16.5 oocytes. Scale bar, 10 μm. (**F**) Immunofluorescence of RPA2 and MEIOB in *Skp1*$^{fl/+}$ and *Skp1*^{cKO} E16.5 oocytes. The plots show the number of RPA2 foci and MEIOB foci, respectively, in oocytes from two embryos per genotype. Scale bar, 10 μm.

of SKP1 in chromosome synapsis is conserved in meiosis in both sexes (49).

Abnormal accumulation of HORMAD1 and HORMAD2 on the chromosome axis in *Skp1*^{cKO} oocytes

To determine whether SKP1 is required for removal of HORMAD1 from chromosome axis in oocytes, we evaluated HORMAD1 in spread nuclei of E16.5 oocytes. As expected, HORMAD1 was absent in SCs in wild type pachytene oocytes. However, HORMAD1 was highly enriched on the chromosome axis in *Skp1*^{cKO} oocytes at the zygotene-like (Supplementary Figure S5D) and pachytene-like stages (Figure 5E). Likewise, HORMAD2 abnormally accumulated on the chromosome axis in zygotene-like and pachytene-like oocytes from E15.5 ovaries (Supplementary Figure S5E). Together with our findings in *Skp1*^{cKO} spermatocytes (Figure 2A), SKP1 restrains HORMAD1 accumulation on the chromosome axis in meiotic germ cells from both sexes.

In contrast with the large foci of RPA2 and MEIOB observed in *Skp1*^{cKO} spermatocytes (Figures 3 and 4A), the sizes of RPA2 and MEIOB foci in the *Skp1*^{cKO} pachytene-like oocytes were comparable with that in the control oocytes (Figure 5F). In addition, these ssDNA-binding proteins did not form thin fibers in *Skp1*^{cKO} oocytes. The number of RPA2 foci was higher in *Skp1*^{cKO} pachytene-like oocytes, whereas the number of MEIOB foci was similar between mutant and control oocytes (Figure 5F). The intensity of IHO1 foci appeared to be comparable between *Skp1*^{cKO} zygotene-like oocytes and wild type zygotene oocytes, however, IHO1 foci persisted in pachytene-like *Skp1*^{cKO} oocytes, in contrast with wild type pachytene oocytes (Supplementary Figure S5F). These results show that meiotic DSB repair defects are less severe in *Skp1*^{cKO} oocytes than spermatocytes.

Reduction of HORMAD1 rescues excessive accumulation of pre-DSB complexes in *Skp1*^{cKO} spermatocytes

HORMAD1 deficiency causes a failure in chromosomal synapsis and a sharp reduction in the formation of meiotic DSBs (33,50). Since HORMAD1 accumulates in *Skp1*^{cKO} spermatocytes, we asked whether HORMAD1 reduction or deficiency rescues meiotic defects in *Skp1*^{cKO} mice. Western blot and immunofluorescence analyses showed that HORMAD1 was reduced in abundance in *Hormad1*$^{+/-}$ testis or spermatocytes and absent in *Hormad1*$^{-/-}$ testis or spermatocytes (Supplementary Figure S6A and B). Histological and nuclear spread analyses revealed that the most advanced spermatocytes in *Skp1*^{cKO}*Hormad1*$^{+/-}$, *Skp1*^{cKO}*Hormad1*$^{-/-}$ or *Skp1*$^{fl/-}$*Hormad1*$^{-/-}$ testes were zygotene-like as in *Skp1*^{cKO} testis (Figure 6A and B). We next examined the localization of RPA2 in *Skp1*$^{fl/+}$, *Skp1*^{cKO}, *Skp1*$^{fl/-}$*Hormad1*$^{-/-}$, *Skp1*^{cKO}*Hormad1*$^{+/-}$, and *Skp1*^{cKO}*Hormad1*$^{-/-}$ spermatocytes and made several observations. First, while large RPA2 foci and RPA2 fibers were still formed in *Skp1*^{cKO}*Hormad1*$^{+/-}$ spermatocytes (Figure 6B), the percentage of spermatocytes with RPA2 fibers was significantly reduced in *Skp1*^{cKO}*Hormad1*$^{+/-}$ testis in comparison with *Skp1*^{cKO} testis (Figure 6C). Second, the number of RPA2 foci in zygotene-like spermatocytes without RPA2 fibers was significantly lower in *Skp1*^{cKO}*Hormad1*$^{+/-}$ testis than *Skp1*^{cKO} testis (Figure 6D). These results indicate that HORMAD1 reduction in *Skp1*^{cKO} spermatocytes lessens the aberrant RPA2 localization in *Skp1*^{cKO} spermatocytes. Third, because DSB formation and early recombination events were disrupted in *Hormad1*$^{-/-}$ testes (33,50), RPA2 foci were dramatically decreased in *Skp1*$^{fl/-}$*Hormad1*$^{-/-}$ leptotene-like spermatocytes compared with the *Skp1*$^{fl/+}$ controls (Figure 6B). In contrast, the RPA2 foci were still higher in number and larger in size in *Skp1*^{cKO}*Hormad1*$^{-/-}$ spermatocytes than in *Skp1*$^{fl/-}$*Hormad1*$^{-/-}$ spermatocytes, indicating that SKP1 might also regulate meiotic DSBs independent of HORMAD1 (Supplementary Figure S6C and D). Furthermore, leptotene-like cells, which had separated sister chromatids, were still present in the *Skp1 Hormad1* double mutants. These results suggest that SKP1 may have multiple roles in meiosis: one that is epistatic to HORMAD1 and another that appears to be independent of HORMAD1.

We investigated the pre-DSB complex components IHO1 and REC114 in spermatocytes from mice of various genotypes. IHO1 and REC114 still formed foci on the chromosome axis in *Skp1*^{cKO}*Hormad1*$^{+/-}$ leptotene cells but with lower intensity than in *Skp1*^{cKO} leptotene cells (Figure 6B). The signal intensity of IHO1 and REC114 was decreased by 64% and 53% respectively in *Skp1*^{cKO}*Hormad1*$^{+/-}$ leptotene cells compared to *Skp1*^{cKO} leptotene-like cells (Figure 6E and F). In addition, the number of IHO1 foci or REC114 foci in *Skp1*^{cKO}*Hormad1*$^{+/-}$ leptotene cells was significantly lower than that in *Skp1*^{cKO} leptotene cells but comparable with that in *Skp1*$^{fl/+}$ cells (Supplementary Figure S6E and F). These results suggest that the reduced HORMAD1 level decreases the pre-DSB complex on the chromosome axis.

HORMAD1 is essential for the formation of the numerous small IHO1 or REC114 foci but dispensable for the few (several) large IHO1 or REC114 blobs, which correspond to the mo-2 minisatellite regions (39). The small foci were nearly absent but the large blobs were still present in *Skp1*^{cKO}*Hormad1*$^{-/-}$ or *Skp1*$^{fl/-}$*Hormad1*$^{-/-}$ spermatocytes (Figure 6B). In addition, these large IHO1 and REC114 blobs were larger in *Skp1*^{cKO}*Hormad1*$^{-/-}$ (double mutant) spermatocytes than in *Skp1*$^{fl/-}$*Hormad1*$^{-/-}$ spermatocytes (Figure 6G and H). Confocal microscopy analysis showed that the large IHO1 blob at mo-2 sites consisted of a cluster of smaller foci (Figure 6I). These results suggest that SKP1 restrains the small IHO1/REC114 foci via HORMAD1 but regulates the large IHO1/REC114 blobs at mo-2 minisatellite regions in a HORMAD1-independent manner.

Reduction of SPO11 fails to rescue defects in meiotic DSBs in *Skp1*-deficient cells

Inactivation of SPO11 leads to a failure in meiotic DSB formation (4,5). The *Spo11* heterozygosity decreases the number of DSBs in wild type (*Atm*$^{+/+}$) mice and in *Atm*$^{-/-}$ mice (25,51). As a result, loss of one *Spo11* allele rescues some meiotic defects in *Atm*$^{-/-}$ mice (52,53). To address whether defects in DSBs in *Skp1*^{cKO} spermatocytes depend on SPO11, we generated *Skp1*^{cKO}*Spo11*$^{+/-}$ mice. *Skp1*^{cKO}*Spo11*$^{+/-}$ spermatocytes showed zygotene-like ar-

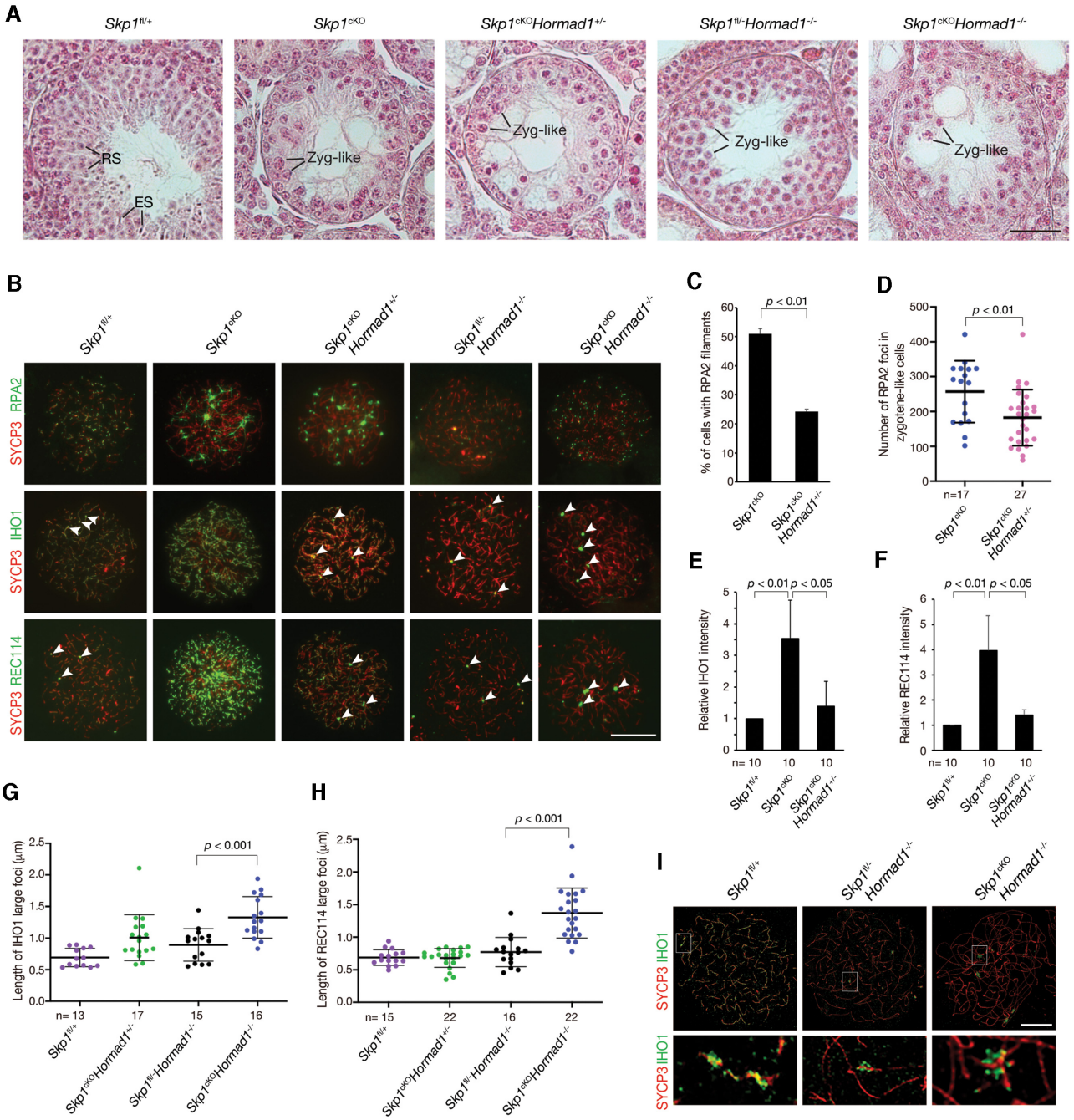

Figure 6. Reduction of HORMAD1 rescues excessive accumulation of pre-DSB complexes in *Skp1*^{cKO} mutant. (**A**) Histology of testes from *Skp1*$^{fl/+}$, *Skp1*^{cKO}, *Skp1*^{cKO}*Hormad1*$^{+/-}$, *Skp1*$^{fl/-}$*Hormad1*$^{-/-}$ and *Skp1*^{cKO}*Hormad1*$^{-/-}$ mice at P30. Zyg-like, zygotene-like spermatocytes; RS, round spermatids; ES, elongated spermatids. Scale bar, 50 μm. (**B**) Immunofluorescence of RPA2, IHO1, and REC114 in leptotene or leptotene-like spermatocytes from P30 testes. White arrowheads indicate the large IHO1 or REC114 blobs, known sites of mo-2 minisatellite arrays (39). Scale bar, 10 μm. (**C**) The percentage of spermatocytes with RPA2 fibers in P30 *Skp1*^{cKO} and *Skp1*^{cKO}*Hormad1*$^{+/-}$ testes. 120–130 cells from two mice per genotype were counted. (**D**) The number of RPA2 foci in zygotene-like cells from P30 *Skp1*^{cKO} and *Skp1*^{cKO}*Hormad1*$^{+/-}$ testes. (E, F) Relative intensity of IHO1 (**E**) and REC114 (**F**) in *Skp1*$^{fl/+}$, *Skp1*^{cKO}, and *Skp1*^{cKO}*Hormad1*$^{+/-}$ leptotene spermatocytes from P30 testes. Fluorescent signals of IHO1 and REC114 were normalized to SYCP3 signal, and the values were set at 1.0 for *Skp1*^{cKO} cells. *n*, number of leptotene cells. (G, H) The diameter of IHO1 blobs (**G**) and REC114 blobs (**H**). These blobs (large foci) correspond to regions of mo-2 minisatellite arrays (39). (**I**) Confocal microscopy of IHO1 and SYCP3 in spermatocytes from P30 *Skp1*$^{fl/+}$, *Skp1*$^{fl/-}$*Hormad1*$^{-/-}$ and *Skp1*^{cKO}*Hormad1*$^{-/-}$ mice. Scale bar, 10 μm. Value = mean ± s.d. The *P* value was calculated by Student's *t*-test.

rest, which was similar to the *Skp1*^{cKO} spermatocytes (Supplementary Figure S7A). As expected, only a few RPA2 foci were observed in *Skp1*$^{fl/+}$*Spo11*$^{-/-}$ spermatocytes (Supplementary Figure S7B). The large RPA2 foci and spider-web like RPA2 fibers were still present in *Skp1*^{cKO}*Spo11*$^{+/-}$ spermatocytes (Supplementary Figure S7B). The percentage of spermatocytes with RPA2 fibers was similar between *Skp1*^{cKO} testes and *Skp1*^{cKO}*Spo11*$^{+/-}$ testes (Supplementary Figure S7C). IHO1 foci were still formed in *Skp1*$^{fl/+}$*Spo11*$^{-/-}$ spermatocytes (Supplementary Figure S7B), which could be explained by the model that the pre-DSB complex (IHO1–REC114–MEI4) functions upstream of SPO11 (Figure 2E) (10). The IHO1 signal intensity was similar between *Skp1*^{cKO} and *Skp1*^{cKO}*Spo11*$^{+/-}$ spermatocytes but was more intense than that in *Skp1*$^{fl/+}$ or *Skp1*$^{fl/+}$*Spo11*$^{-/-}$ spermatocytes (Supplementary Figure S7B). These results demonstrate that reduction of SPO11 does not ameliorate the DSB defects in *Skp1*^{cKO} spermatocytes.

SCF-FBXO47 targets HORMAD1 for ubiquitination and degradation

In the SCF complex, SKP1 binds to an F-box protein through the conserved 40-aa F-box domain (27,29). The F-box family of proteins provides substrate specificity for ubiquitination by the SCF complex. HORMAD1 accumulates dramatically on synapsed SC in *Skp1*-deficient pachytene cells from the inducible *Skp1* mutant (30). The abundance of HORMAD1 on unsynapsed chromosome axis in *Skp1*^{cKO} spermatocytes was increased by three folds (Figure 2A). Thus, SKP1 could inhibit accumulation of HORMAD1 on both synapsed and unsynapsed SCs in *Skp1* mutant spermatocytes through the same mechanism. To identify the F-box proteins that recognize HORMAD1, we chose several potential candidates: FBXW8, FBXW17, FBXO28 and FBXO47, because peptides of FBXW8, FBXW17, and FBXO28 were present in the same mass spectrometry dataset that identified SKP1 and HORMAD1 (18) and FBXO47-deficient mice showed meiotic arrest (54,55). F-box proteins physically interact with their substrate proteins (56). We performed co-transfections to express epitope-tagged proteins in HEK293T cells. SKP1, FBXW8, FBXW17, and FBXO28 are ubiquitously expressed and thus are expected to be present in HEK293T cells. FBXO47 and HORMAD1 are meiosis-specific and thus are expected to be absent in HEK293T cells (33,54,57). We tested the interaction of HORMAD1 with these four candidate F-box proteins by co-transfection in HEK293T cells followed by co-immunoprecipitation. HORMAD1 was complexed with FBXO47 but not with FBXW8, FBXW17 or FBXO28 (Figure 7A–D). As expected, SKP1 was associated with F-box proteins such as FBXO28 and FBXO47 (Figure 7E, F).

To test whether HORMAD1 is ubiquitinated by the SCF ubiquitin E3 ligase, we transfected HEK293T cells with constructs expressing HA-ubiquitin, V5-HORMAD1 and one of the following F-box proteins: FBXW8, FBXW17, FBXO28 and FBXO47 (Figure 7G). V5-HORMAD1 was immunoprecipitated with the anti-V5 antibody and subjected to Western blotting with anti-HA antibody to detect poly-ubiquitinated isoforms. We detected poly-ubiquitinated protein species in the presence of FBXO47 but not any of the other three F-box proteins examined (Figure 7G). As expected, the band intensity of HORMAD1 (non-ubiquitinated) in the FBXO47 lane was much lower than in other lanes, suggesting that the majority of HORMAD1 was polyubiquitinated (Figure 7G). These results demonstrate that FBXO47 recognizes and targets HORMAD1 for poly-ubiquitination.

DISCUSSION

SKP1 is an evolutionarily conserved core subunit of the SCF ubiquitin E3 ligases and functions as an adaptor in these holoenzyme complexes (27). Some species such as mouse, human, and yeast have only one *Skp1* gene, while others, such as *C. elegans*, *Arabidopsis* and *Drosophila* have multiple *Skp1* homologues (up to 21) due to gene duplications (58,59,60). Functionally, zygotic knockdown of *Skr1-1/2* (two closely related *Skp1* homologues) in *C. elegans* results in meiotic arrest (58) and one of the *Skp1*-related genes (*Ask1*) in *Arabidopsis* is essential for male meiosis (61). A temperature-sensitive *Skp1* fission yeast mutant exhibits abnormal spindle bending in meiosis I and defects in resolution of meiotic recombination intermediates (62). Yeast and *Drosophila* SCF regulates SC assembly (60,63). In mice, inducible depletion of SKP1 in meiotic cells reveals an essential role for SKP1 in the maintenance of chromosomal synapsis and the metaphase to prophase transition during meiosis I (30). In this study, we demonstrate that SKP1 plays crucial and distinct roles in DSB homeostasis, synapsis initiation, and sister chromatid cohesion in early meiosis in mice. These studies support that SKP1/SCF regulates multiple key molecular processes in meiosis in sexually reproducing organisms.

The ATM kinase is essential for meiosis (23,24) and *Atm*-deficient spermatocytes display both synapsis failure and increased DSBs (10 times more DSBs) in mice (12,22,23,24,25,26). The role of ATM (its yeast homologue Tel1) in control of the meiotic DSB number is conserved in budding yeast (64,65). The *Spo11* heterozygosity reduces the number of DSBs in otherwise wild type mice (51). Likewise, the number of meiotic DSBs is reduced in *Atm*$^{-/-}$*Spo11*$^{+/-}$ mice in comparison with *Atm*$^{-/-}$ mice (25). In mice, chromosomal synapsis and meiotic recombination are inter-dependent. Notably, chromosomal synapsis is restored in *Atm*$^{-/-}$*Spo11*$^{+/-}$ mice (52,53), suggesting that the synapsis failure in *Atm*$^{-/-}$ mice is most likely to be a secondary effect of altered DSB homeostasis (25). Thus, the synapsis failure in *Skp1*^{cKO} germ cells could also be due to defective DSB homeostasis. However, *Spo11* heterozygosity could not rescue the synapsis failure in *Skp1*^{cKO} germ cells, suggesting a different underlying mechanism. While ATM restrains DSB formation (12,25), HORMAD1 does not accumulate excessively on the chromosome axis in *Atm*$^{-/-}$ spermatocytes (57), indicating that ATM may not function through HORMAD1. In contrast, in *Skp1*^{cKO} meiotic cells, HORMAD1 accumulates dramatically on the chromosome axis, with concurrent accumulation of pre-DSB (IHO1–REC114–MEI4) complexes. Moreover, *Hormad1* heterozygosity reduces the number and intensity of foci of RPA2 and

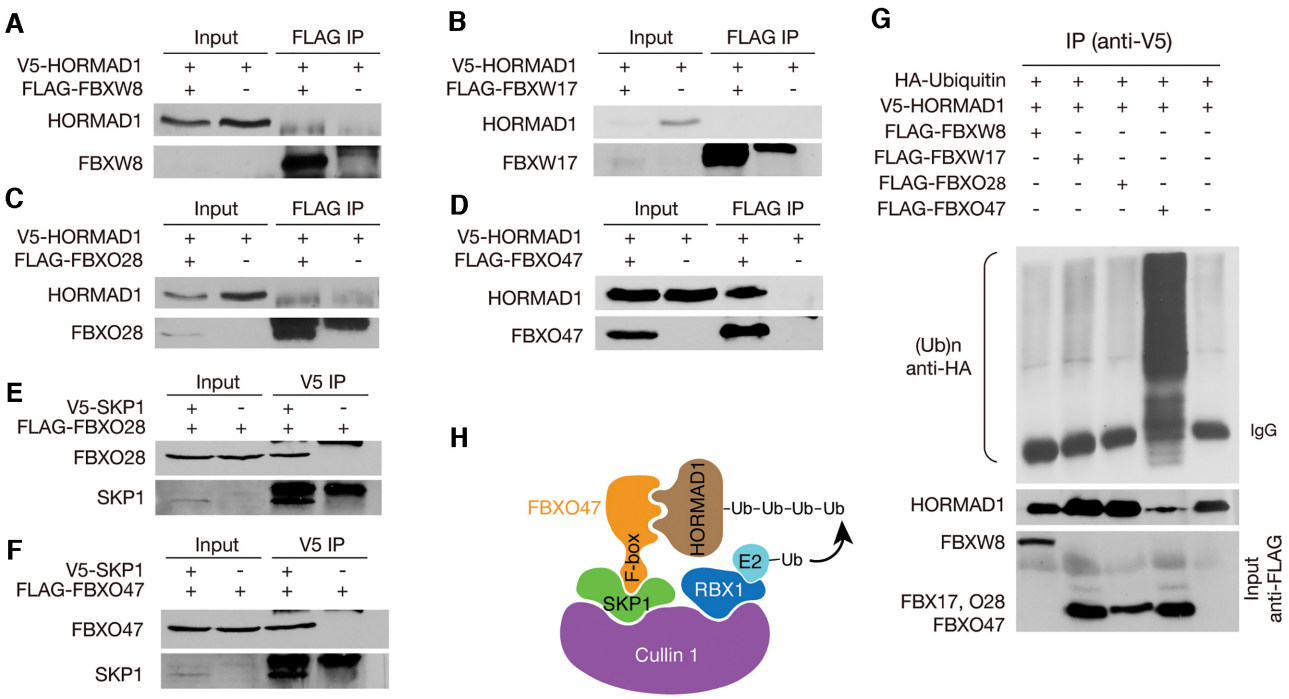

Figure 7. FBXO47 interacts with and targets HORMAD1 for polyubiquitination. (A–D) Co-immunoprecipitation analyses of HORMAD1 with FBXW8 (**A**), FBXW17 (**B**), FBXO28 (**C**) and FBXO47 (**D**) in HEK293T cells. (E, F) Co-immunoprecipitation analyses of SKP1 with FBXO28 (**E**) and FBXO47 (**F**) in HEK293T cells. (**G**) Polyubiquitination assays of HORMAD1 in the presence of FBXW8, FBXW17, FBXO28 or FBXO47. All co-transfections were performed in HEK293T cells and the experiments were performed twice (A–G). (**H**) A working model for ubiquitination-mediated degradation of HORMAD1. FBXO47 interacts with both SKP1 and HORMAD1. Cullin1 is a scaffold protein for the SCF complex. RBX1 recruits an E2 enzyme.

pre-DSB components in *Skp1*^{cKO} spermatocytes. We propose a working model in which SKP1-dependent regulation of HORMAD1 levels on the chromosome axis contributes to DSB homeostasis (Figure 2E). These studies suggest that the SCF ubiquitin E3 ligase and the ATM kinase regulate meiotic DSB homeostasis through distinct mechanisms.

The abnormal localization of DSB repair proteins in *Skp1*^{cKO} spermatocytes suggests that SKP1 may act to prevent excessive formation of DSBs and/or end resection. The DSB repair proteins exhibit unusually large foci and long thin threads in *Skp1*^{cKO} spermatocytes (Figures 3 and 4). Such phenotypes are not known in any other mouse meiotic mutants. We postulate that the unusually large size of RPA foci in *Skp1*^{cKO} spermatocytes might be caused by formation of multiple DSBs in proximity. In wild type meiotic cells, the average length of the ssDNA after DSB end resection is about 1 kb (11,12). The long RPA thin threads in *Skp1*^{cKO} spermatocytes may represent super long ssDNA, which could be generated by defective DSB end resection.

SCF regulates the SC assembly and meiotic recombination in diverse species. In budding yeast, depletion of *Cdc53* (cullin) or the *Cdc4* (an F-box protein) mutation causes defects in the SC assembly (63). In rice, F-box proteins MOF and ZYGO1 mediates homologue pairing, synapsis, and meiotic DSB processing (66,67). In *Drosophila* female meiosis, SkpA regulates the SC formation and maintenance through FBXO42-mediated downregulation of the phosphatase subunit PP2A-B56 (60). Mouse HORMAD1 is essential for both chromosomal synapsis and meiotic recombination (33,50). In this study, conditional inactivation of SKP1 using the *Stra8*-Cre prior to meiosis demonstrates that SKP1 is required for initiation of chromosomal synapsis. In mice, HORMAD1 is present on unsynapsed but not on synapsed chromosome axes. Eviction of HORMAD1 appears to be a pre-requisite for synapsis. In *Skp1*^{cKO} meiotic germ cells, the failure in chromosomal synapsis is likely caused by the accumulation and persistence of HORMAD1 on the chromosome axis. Notably, HORMAD1 also accumulates on the chromosome axis in *Trip13* mutant spermatocytes (57). Although the *Trip13* mutant spermatocytes showed substantial homologue synapsis, they still displayed asynapsis at centromeric chromosome ends and some interstitial asynapsis (68,69). Therefore, the synapsis defects were still present in *Trip13* mutant spermatocytes but less severe than in the *Skp1*^{cKO} spermatocytes. There are two possible explanations for the difference in the severity of synapsis defects between these two mutants. First, the level of HORMAD1 accumulation on the chromosome axis appears to be much higher in *Skp1*^{cKO} mutant than in *Trip13* mutant cells. Second, the *Trip13* mutant allele in the *Trip13* studies was a gene-trap allele and thus could be a hypomorphic allele rather than a null allele (57,68,69). Co-transfections in HEK293T cells show that SCF-FBXO47 targets HORMAD1 for polyubiquitination. However, FBXO47 is unlikely to be the sole F-box protein required for chromosomal synapsis in mice, since *Skp1*^{cKO} spermatocytes completely lack synapsis but the FBXO47-deficient spermatocytes still display substantial synapsis, indicating that additional F-box proteins are involved (54,55). *C. elegans* Prom-1 is a homologue of FBXO47. The SCF–Prom-1 E3 ligase

downregulates mitotic cell cycle regulators at meiotic entry (70). While these studies support an evolutionarily conserved role for the SCF ubiquitin E3 ligase in SC assembly, they also underscore the complexity of the SCF functions in meiosis. There are 69 mammalian F-box proteins (28). SKP1 plays multiple roles in meiosis in mice. It is possible that different F-box proteins may be involved in synapsis formation, DSB homeostasis, and sister chromatid cohesion. It is also possible that SKP1 may function in some aspects of meiosis independent of the SCF complex.

Sister chromatid cohesion is established during DNA replication. During meiotic prophase I, the chromosome axes form axial elements consisting of cohesins, HORMA-domain proteins, and axial synaptonemal complex proteins (71). Axial elements are important for chromosomal synapsis and meiotic recombination. REC8, a meiosis-specific cohesin, ensures synapsis between chromosome homologues rather than between sister chromatids (36,38,72). We find that depletion of SKP1 causes defective sister chromatid cohesion in leptotene-like spermatocytes. Meiosis-specific cohesins (REC8 and STAG3) and the SC proteins still localize to the axial cores of the separated sister chromatids in *Skp1*^{cKO} leptotene-like cells. These observations suggest that SCF plays a key role in sister chromatid cohesion but the mechanism remains unknown. There are several possibilities. First, SCF targets many cell cycle drivers such as cyclins and thus is a key regulator of the cell cycle progression (73). It is possible that delayed meiotic entry may contribute to defective sister chromatid cohesion in *Skp1*^{cKO} leptotene-like cells. Second, SCF may directly target regulators of sister chromatid cohesion. Third, sister chromatid cohesion appears to be intact in the majority of *Skp1*^{cKO} spermatocytes (leptotene and zygotene-like). The intact sister chromatid cohesion may be attributed to a possible delayed depletion of the SKP1 protein in these conditional knockout cells. Regardless of mechanisms, defects in sister chromatid cohesion could affect chromatin loop formation, DSB formation and processing. Sister chromatid cohesion is coupled with the pre-meiotic S phase DNA replication, which in turn is directly linked with recombination initiation (74,75,76). Therefore, we postulate that the SCF ubiquitin E3 ligase plays a key role in the coordination of sister chromatid cohesion, meiotic DNA replication, and DSB processing.

Although male and female *Skp1*^{cKO} germ cells exhibit similar meiotic defects: a failure in synapsis, a failure in meiotic recombination, and excessive accumulation of HORMAD1 on the chromosome axis, they also have differences. First, the synaptic defect is less severe in *Skp1*^{cKO} oocytes, which still display limited synapsis. In contrast, the *Skp1*^{cKO} spermatocytes completely lack synapsis. Second, defects in sister chromatid cohesion are present in *Skp1*^{cKO} spermatocytes but not in *Skp1*^{cKO} oocytes. Third, meiotic recombination defects are less severe in mutant oocytes than in mutant spermatocytes. The large foci and long thin threads of DSB repair proteins such as RPA are present in *Skp1*^{cKO} spermatocytes but not in oocytes. Lastly, pre-DSB complex components accumulate excessively only in *Skp1*^{cKO} spermatocytes. The difference in the severity of meiotic defects between *Skp1*^{cKO} males and females could be due to the differential duration of SKP1 deletion before meiotic initiation in males and females. In males, *Stra8*-Cre is expressed at postnatal day three, seven days before meiotic initiation, which allows SKP1 to be efficiently depleted before germ cells enter meiosis (Supplementary Figure S1) (34,35). In contrast, *Stra8*-Cre is expressed at E12.5 in females, one day before meiotic onset, leaving less time for SKP1 to be depleted before meiotic prophase I (Supplementary Figure S1). However, the sex-specific differences in meiotic defects in *Skp1*^{cKO} mice could also be due to sexual dimorphism of meiosis itself (77).

SUPPLEMENTARY DATA

Supplementary Data are available at NAR Online.

ACKNOWLEDGEMENTS

We thank Aleksandar Rajkovic for HORMAD1 antibody, Attila Toth for IHO1, MEI4, HORMAD2 antibodies, Scott Keeney for anti-REC114 antibody, Hiroki Shibuya for BRME1 and HSF2BP antibodies, Richard Schultz for YBX2 antibody, and José Luis Barbero for STAG3 antibody. We thank Jessica Chotiner and Fang Yang for comments on the manuscript.

FUNDING

NIH/National Institute of Child Health and Human Development [HD069592 and HD068157 to P.J.W.]; NIH/National Cancer Institute [R01CA207513 to L.B.; R01CA240814 to S.Y.F.]; National Natural Science Foundation of China [31771588 to M.L.]. Funding for open access charge: NIH.
Conflict of interest statement. None declared.

REFERENCES

1. Zickler,D. and Kleckner,N. (1999) Meiotic chromosomes: integrating structure and function. *Annu. Rev. Genet.*, **33**, 603–754.
2. Page,S.L. and Hawley,R.S. (2004) The genetics and molecular biology of the synaptonemal complex. *Annu. Rev. Cell Dev. Biol.*, **20**, 525–558.
3. Handel,M.A. and Schimenti,J.C. (2010) Genetics of mammalian meiosis: regulation, dynamics and impact on fertility. *Nat. Rev. Genet.*, **11**, 124–136.
4. Romanienko,P.J. and Camerini-Otero,R.D. (2000) The mouse spo11 gene is required for meiotic chromosome synapsis. *Mol. Cell*, **6**, 975–987.
5. Baudat,F., Manova,K., Yuen,J.P., Jasin,M. and Keeney,S. (2000) Chromosome synapsis defects and sexually dimorphic meiotic progression in mice lacking spo11. *Mol. Cell*, **6**, 989–998.
6. Robert,T., Nore,A., Brun,C., Maffre,C., Crimi,B., Bourbon,H.M. and de Massy,B. (2016) The topovib-like protein family is required for meiotic DNA double-strand break formation. *Science*, **351**, 943–949.
7. Mihola,O., Trachtulec,Z., Vlcek,C., Schimenti,J.C. and Forejt,J. (2009) A mouse speciation gene encodes a meiotic histone H3 methyltransferase. *Science*, **323**, 373–375.
8. Parvanov,E.D., Petkov,P.M. and Paigen,K. (2010) Prdm9 controls activation of mammalian recombination hotspots. *Science*, **327**, 835.
9. Baudat,F., Buard,J., Grey,C., Fledel-Alon,A., Ober,C., Przeworski,M., Coop,G. and de Massy,B. (2010) PRDM9 is a major determinant of meiotic recombination hotspots in humans and mice. *Science*, **327**, 836–840.
10. Stanzione,M., Baumann,M., Papanikos,F., Dereli,I., Lange,J., Ramlal,A., Trankner,D., Shibuya,H., de Massy,B., Watanabe,Y. *et al.* (2016) Meiotic DNA break formation requires the unsynapsed chromosome axis-binding protein IHO1 (CCDC36) in mice. *Nat. Cell Biol.*, **18**, 1208–1220.

11. Wold,M.S. (1997) Replication protein A: a heterotrimeric, single-stranded DNA-binding protein required for eukaryotic DNA metabolism. *Annu. Rev. Biochem.*, **66**, 61–92.
12. Lange,J., Yamada,S., Tischfield,S.E., Pan,J., Kim,S., Zhu,X., Socci,N.D., Jasin,M. and Keeney,S. (2016) The landscape of mouse meiotic double-strand break formation, processing, and repair. *Cell*, **167**, 695–708.
13. Bishop,D.K. (1994) RecA homologs dmc1 and rad51 interact to form multiple nuclear complexes prior to meiotic chromosome synapsis. *Cell*, **79**, 1081–1092.
14. Hinch,A.G., Becker,P.W., Li,T., Moralli,D., Zhang,G., Bycroft,C., Green,C., Keeney,S., Shi,Q., Davies,B. *et al.* (2020) The configuration of RPA, RAD51, and DMC1 binding in meiosis reveals the nature of critical recombination intermediates. *Mol. Cell*, **79**, 689–701.
15. Brandsma,I., Sato,K., van Rossum-Fikkert,S.E., van Vliet,N., Sleddens,E., Reuter,M., Odijk,H., van den Tempel,N., Dekkers,D.H.W., Bezstarosti,K. *et al.* (2019) HSF2BP interacts with a conserved domain of BRCA2 and is required for mouse spermatogenesis. *Cell. Rep.*, **27**, 3790–3798.
16. Zhang,J., Fujiwara,Y., Yamamoto,S. and Shibuya,H. (2019) A meiosis-specific BRCA2 binding protein recruits recombinases to DNA double-strand breaks to ensure homologous recombination. *Nat. Commun.*, **10**, 722.
17. Takemoto,K., Tani,N., Takada-Horisawa,Y., Fujimura,S., Tanno,N., Yamane,M., Okamura,K., Sugimoto,M., Araki,K. and Ishiguro,K.I. (2020) Meiosis-specific C19orf57/4930432K21Rik/BRME1 modulates localization of RAD51 and DMC1 to DSBs in mouse meiotic recombination. *Cell. Rep.*, **31**, 107686.
18. Luo,M., Yang,F., Leu,N.A., Landaiche,J., Handel,M.A., Benavente,R., La Salle,S. and Wang,P.J. (2013) MEIOB exhibits single-stranded DNA-binding and exonuclease activities and is essential for meiotic recombination. *Nat. Commun.*, **4**, 2788.
19. Souquet,B., Abby,E., Herve,R., Finsterbusch,F., Tourpin,S., Le Bouffant,R., Duquenne,C., Messiaen,S., Martini,E., Bernardino-Sgherri,J. *et al.* (2013) MEIOB targets single-strand DNA and is necessary for meiotic recombination. *PLoS Genet.*, **9**, e1003784.
20. Xu,Y., Greenberg,R.A., Schonbrunn,E. and Wang,P.J. (2017) Meiosis-specific proteins MEIOB and SPATA22 cooperatively associate with the ssDNA-binding RPA complex and DNA double-strand breaks. *Biol. Reprod.*, **96**, 1096–1104.
21. Guo,R., Xu,Y., Leu,N.A., Zhang,L., Fuchs,S.Y., Ye,L. and Wang,P.J. (2020) The ssDNA-binding protein MEIOB acts as a dosage-sensitive regulator of meiotic recombination. *Nucleic Acids Res.*, **48**, 12219–12233.
22. Lukaszewicz,A., Lange,J., Keeney,S. and Jasin,M. (2018) Control of meiotic double-strand-break formation by ATM: local and global views. *Cell. Cycle*, **17**, 1155–1172.
23. Xu,Y., Ashley,T., Brainerd,E.E., Bronson,R.T., Meyn,M.S. and Baltimore,D. (1996) Targeted disruption of ATM leads to growth retardation, chromosomal fragmentation during meiosis, immune defects, and thymic lymphoma. *Genes Dev.*, **10**, 2411–2422.
24. Plug,A.W., Peters,A.H., Xu,Y., Keegan,K.S., Hoekstra,M.F., Baltimore,D., de Boer,P. and Ashley,T. (1997) ATM and RPA in meiotic chromosome synapsis and recombination. *Nat. Genet.*, **17**, 457–461.
25. Lange,J., Pan,J., Cole,F., Thelen,M.P., Jasin,M. and Keeney,S. (2011) ATM controls meiotic double-strand-break formation. *Nature*, **479**, 237–240.
26. Paiano,J., Wu,W., Yamada,S., Sciascia,N., Callen,E., Paola Cotrim,A., Deshpande,R.A., Maman,Y., Day,A., Paull,T.T. *et al.* (2020) ATM and PRDM9 regulate SPO11-bound recombination intermediates during meiosis. *Nat. Commun.*, **11**, 857.
27. Cardozo,T. and Pagano,M. (2004) The SCF ubiquitin ligase: insights into a molecular machine. *Nat. Rev. Mol. Cell Biol.*, **5**, 739–751.
28. Reitsma,J.M., Liu,X., Reichermeier,K.M., Moradian,A., Sweredoski,M.J., Hess,S. and Deshaies,R.J. (2017) Composition and regulation of the cellular repertoire of SCF ubiquitin ligases. *Cell*, **171**, 1326–1339.
29. Nguyen,K.M. and Busino,L. (2020) The biology of F-box proteins: the SCF family of E3 ubiquitin ligases. *Adv. Exp. Med. Biol.*, **1217**, 111–122.
30. Guan,Y., Leu,N.A., Ma,J., Chmatal,L., Ruthel,G., Bloom,J.C., Lampson,M.A., Schimenti,J.C., Luo,M. and Wang,P.J. (2020) SKP1 drives the prophase i to metaphase i transition during male meiosis. *Sci. Adv.*, **6**, eaaz2129.
31. Bai,C., Sen,P., Hofmann,K., Ma,L., Goebl,M., Harper,J.W. and Elledge,S.J. (1996) SKP1 connects cell cycle regulators to the ubiquitin proteolysis machinery through a novel motif, the F-box. *Cell*, **86**, 263–274.
32. Hayashi,K., Yoshida,K. and Matsui,Y. (2005) A histone H3 methyltransferase controls epigenetic events required for meiotic prophase. *Nature*, **438**, 374–378.
33. Shin,Y.H., Choi,Y., Erdin,S.U., Yatsenko,S.A., Kloc,M., Yang,F., Wang,P.J., Meistrich,M.L. and Rajkovic,A. (2010) Hormad1 mutation disrupts synaptonemal complex formation, recombination, and chromosome segregation in mammalian meiosis. *PLoS Genet.*, **6**, e1001190.
34. Lin,Z., Hsu,P.J., Xing,X., Fang,J., Lu,Z., Zou,Q., Zhang,K.J., Zhang,X., Zhou,Y., Zhang,T. *et al.* (2017) Mettl3-/Mettl14-mediated mRNA N(6)-methyladenosine modulates murine spermatogenesis. *Cell Res.*, **27**, 1216–1230.
35. Menke,D.B., Koubova,J. and Page,D.C. (2003) Sexual differentiation of germ cells in XX mouse gonads occurs in an anterior-to-posterior wave. *Dev. Biol.*, **262**, 303–312.
36. Watanabe,Y. and Nurse,P. (1999) Cohesin rec8 is required for reductional chromosome segregation at meiosis. *Nature*, **400**, 461–464.
37. Prieto,I., Suja,J.A., Pezzi,N., Kremer,L., Martinez-A,C., Rufas,J.S. and Barbero,J.L. (2001) Mammalian STAG3 is a cohesin specific to sister chromatid arms in meiosis I. *Nat. Cell Biol.*, **3**, 761–766.
38. Klein,F., Mahr,P., Galova,M., Buonomo,S.B., Michaelis,C., Nairz,K. and Nasmyth,K. (1999) A central role for cohesins in sister chromatid cohesion, formation of axial elements, and recombination during yeast meiosis. *Cell*, **98**, 91–103.
39. Acquaviva,L., Boekhout,M., Karasu,M.E., Brick,K., Pratto,F., Li,T., van Overbeek,M., Kauppi,L., Camerini-Otero,R.D., Jasin,M. *et al.* (2020) Ensuring meiotic DNA break formation in the mouse pseudoautosomal region. *Nature*, **582**, 426–431.
40. Burma,S., Chen,B.P., Murphy,M., Kurimasa,A. and Chen,D.J. (2001) ATM phosphorylates histone H2AX in response to DNA double-strand breaks. *J. Biol. Chem.*, **276**, 42462–42467.
41. La Salle,S., Palmer,K., O'Brien,M., Schimenti,J.C., Eppig,J. and Handel,M.A. (2012) Spata22, a novel vertebrate-specific gene, is required for meiotic progress in mouse germ cells. *Biol. Reprod.*, **86**, 45.
42. Yoshida,K., Kondoh,G., Matsuda,Y., Habu,T., Nishimune,Y. and Morita,T. (1998) The mouse reca-like gene dmc1 is required for homologous chromosome synapsis during meiosis. *Mol. Cell*, **1**, 707–718.
43. Pittman,D.L., Cobb,J., Schimenti,K.J., Wilson,L.A., Cooper,D.M., Brignull,E., Handel,M.A. and Schimenti,J.C. (1998) Meiotic prophase arrest with failure of chromosome synapsis in mice deficient for dmc1, a germline-specific RecA homolog. *Mol. Cell*, **1**, 697–705.
44. Gallardo,T., Shirley,L., John,G.B. and Castrillon,D.H. (2007) Generation of a germ cell-specific mouse transgenic cre line, vasa-cre. *Genesis*, **45**, 413–417.
45. Yang,J., Medvedev,S., Yu,J., Tang,L.C., Agno,J.E., Matzuk,M.M., Schultz,R.M. and Hecht,N.B. (2005) Absence of the DNA-/RNA-binding protein MSY2 results in male and female infertility. *Proc. Natl. Acad. Sci. U.S.A.*, **102**, 5755–5760.
46. Di Giacomo,M., Barchi,M., Baudat,F., Edelmann,W., Keeney,S. and Jasin,M. (2005) Distinct DNA-damage-dependent and -independent responses drive the loss of oocytes in recombination-defective mouse mutants. *Proc. Natl. Acad. Sci. U.S.A.*, **102**, 737–742.
47. Bolcun-Filas,E., Hall,E., Speed,R., Taggart,M., Grey,C., de Massy,B., Benavente,R. and Cooke,H.J. (2009) Mutation of the mouse syce1 gene disrupts synapsis and suggests a link between synaptonemal complex structural components and DNA repair. *PLoS Genet.*, **5**, e1000393.
48. Hamer,G., Gell,K., Kouznetsova,A., Novak,I., Benavente,R. and Hoog,C. (2006) Characterization of a novel meiosis-specific protein within the central element of the synaptonemal complex. *J. Cell. Sci.*, **119**, 4025–4032.
49. de Vries,F.A., de Boer,E., van den Bosch,M., Baarends,W.M., Ooms,M., Yuan,L., Liu,J.G., van Zeeland,A.A., Heyting,C. and Pastink,A. (2005) Mouse sycp1 functions in synaptonemal complex

assembly, meiotic recombination, and XY body formation. *Genes Dev.*, **19**, 1376–1389.
50. Daniel,K., Lange,J., Hached,K., Fu,J., Anastassiadis,K., Roig,I., Cooke,H.J., Stewart,A.F., Wassmann,K., Jasin,M. *et al.* (2011) Meiotic homologue alignment and its quality surveillance are controlled by mouse HORMAD1. *Nat. Cell Biol.*, **13**, 599–610.
51. Cole,F., Kauppi,L., Lange,J., Roig,I., Wang,R., Keeney,S. and Jasin,M. (2012) Homeostatic control of recombination is implemented progressively in mouse meiosis. *Nat. Cell Biol.*, **14**, 424–430.
52. Bellani,M.A., Romanienko,P.J., Cairatti,D.A. and Camerini-Otero,R.D. (2005) SPO11 is required for sex-body formation, and spo11 heterozygosity rescues the prophase arrest of atm-/- spermatocytes. *J. Cell. Sci.*, **118**, 3233–3245.
53. Barchi,M., Roig,I., Di Giacomo,M., de Rooij,D.G., Keeney,S. and Jasin,M. (2008) ATM promotes the obligate XY crossover and both crossover control and chromosome axis integrity on autosomes. *PLoS Genet.*, **4**, e1000076.
54. Hua,R., Wei,H., Liu,C., Zhang,Y., Liu,S., Guo,Y., Cui,Y., Zhang,X., Guo,X., Li,W. *et al.* (2019) FBXO47 regulates telomere-inner nuclear envelope integration by stabilizing TRF2 during meiosis. *Nucleic Acids Res.*, **47**, 11755–11770.
55. Tanno,N., Takemoto,K., Takada-Horisawa,Y., Shimada,R., Fujimura,S., Tani,N., Takeda,N., Araki,K. and Ishiguro,K.I. (2022) FBXO47 is essential for preventing the synaptonemal complex from premature disassembly in mouse male meiosis. *Iscience*, **25**, 104008.
56. Busino,L., Bassermann,F., Maiolica,A., Lee,C., Nolan,P.M., Godinho,S.I., Draetta,G.F. and Pagano,M. (2007) SCFFbxl3 controls the oscillation of the circadian clock by directing the degradation of cryptochrome proteins. *Science*, **316**, 900–904.
57. Wojtasz,L., Daniel,K., Roig,I., Bolcun-Filas,E., Xu,H., Boonsanay,V., Eckmann,C.R., Cooke,H.J., Jasin,M., Keeney,S. *et al.* (2009) Mouse HORMAD1 and HORMAD2, two conserved meiotic chromosomal proteins, are depleted from synapsed chromosome axes with the help of TRIP13 AAA-ATPase. *PLoS Genet.*, **5**, e1000702.
58. Nayak,S., Santiago,F.E., Jin,H., Lin,D., Schedl,T. and Kipreos,E.T. (2002) The caenorhabditis elegans Skp1-related gene family: diverse functions in cell proliferation, morphogenesis, and meiosis. *Curr. Biol.*, **12**, 277–287.
59. Zhao,D., Ni,W., Feng,B., Han,T., Petrasek,M.G. and Ma,H. (2003) Members of the arabidopsis-SKP1-like gene family exhibit a variety of expression patterns and may play diverse roles in arabidopsis. *Plant Physiol.*, **133**, 203–217.
60. Barbosa,P., Zhaunova,L., Debilio,S., Steccanella,V., Kelly,V., Ly,T. and Ohkura,H. (2021) SCF-Fbxo42 promotes synaptonemal complex assembly by downregulating PP2A-B56. *J. Cell Biol.*, **220**, e202009167.
61. Yang,M., Hu,Y., Lodhi,M., McCombie,W.R. and Ma,H. (1999) The arabidopsis SKP1-LIKE1 gene is essential for male meiosis and may control homologue separation. *Proc. Natl. Acad. Sci. U.S.A.*, **96**, 11416–11421.
62. Okamoto,S.Y., Sato,M., Toda,T. and Yamamoto,M. (2012) SCF ensures meiotic chromosome segregation through a resolution of meiotic recombination intermediates. *PLoS One*, **7**, e30622.
63. Zhu,Z., Bani Ismail,M., Shinohara,M. and Shinohara,A. (2020) SCF(Cdc4) ubiquitin ligase regulates synaptonemal complex formation during meiosis. *Life. Sci. Alliance*, **4**, e202000933.
64. Carballo,J.A., Panizza,S., Serrentino,M.E., Johnson,A.L., Geymonat,M., Borde,V., Klein,F. and Cha,R.S. (2013) Budding yeast ATM/ATR control meiotic double-strand break (DSB) levels by down-regulating rec114, an essential component of the DSB-machinery. *PLoS Genet.*, **9**, e1003545.
65. Mohibullah,N. and Keeney,S. (2017) Numerical and spatial patterning of yeast meiotic DNA breaks by tel1. *Genome Res.*, **27**, 278–288.
66. He,Y., Wang,C., Higgins,J.D., Yu,J., Zong,J., Lu,P., Zhang,D. and Liang,W. (2016) MEIOTIC F-BOX is essential for male meiotic DNA double-strand break repair in rice. *Plant Cell*, **28**, 1879–1893.
67. Zhang,F., Tang,D., Shen,Y., Xue,Z., Shi,W., Ren,L., Du,G., Li,Y. and Cheng,Z. (2017) The F-box protein ZYGO1 mediates bouquet formation to promote homologous pairing, synapsis, and recombination in rice meiosis. *Plant Cell*, **29**, 2597–2609.
68. Li,X.C. and Schimenti,J.C. (2007) Mouse pachytene checkpoint 2 (trip13) is required for completing meiotic recombination but not synapsis. *PLos Genet.*, **3**, e130.
69. Roig,I., Dowdle,J.A., Toth,A., de Rooij,D.G., Jasin,M. and Keeney,S. (2010) Mouse TRIP13/PCH2 is required for recombination and normal higher-order chromosome structure during meiosis. *PLoS Genet.*, **6**, e1001062.
70. Mohammad,A., Vanden Broek,K., Wang,C., Daryabeigi,A., Jantsch,V., Hansen,D. and Schedl,T. (2018) Initiation of meiotic development is controlled by three post-transcriptional pathways in caenorhabditis elegans. *Genetics*, **209**, 1197–1224.
71. Grey,C. and de Massy,B. (2021) Chromosome organization in early meiotic prophase. *Front. Cell. Dev. Biol.*, **9**, 688878.
72. Xu,H., Beasley,M.D., Warren,W.D., van der Horst,G.T. and McKay,M.J. (2005) Absence of mouse REC8 cohesin promotes synapsis of sister chromatids in meiosis. *Dev. Cell.*, **8**, 949–961.
73. Jang,S.M., Redon,C.E., Thakur,B.L., Bahta,M.K. and Aladjem,M.I. (2020) Regulation of cell cycle drivers by cullin-RING ubiquitin ligases. *Exp. Mol. Med.*, **52**, 1637–1651.
74. Borde,V., Goldman,A.S. and Lichten,M. (2000) Direct coupling between meiotic DNA replication and recombination initiation. *Science*, **290**, 806–809.
75. Murakami,H. and Keeney,S. (2014) Temporospatial coordination of meiotic DNA replication and recombination via DDK recruitment to replisomes. *Cell*, **158**, 861–873.
76. Pratto,F., Brick,K., Cheng,G., Lam,K.G., Cloutier,J.M., Dahiya,D., Wellard,S.R., Jordan,P.W. and Camerini-Otero,R.D. (2021) Meiotic recombination mirrors patterns of germline replication in mice and humans. *Cell*, **184**, 4251–4267.
77. Hunt,P.A. and Hassold,T.J. (2002) Sex matters in meiosis. *Science*, **296**, 2181–2183.
78. Zhou,J., Stein,P., Leu,N.A., Chmatal,L., Xue,J., Ma,J., Huang,X., Lampson,M.A., Schultz,R.M. and Wang,P.J. (2015) Accelerated reproductive aging in females lacking a novel centromere protein SYCP2L. *Hum. Mol. Genet.*, **24**, 6505–6514.